

Electrochemical Filtration of Gadolinium from Patient Urine after Magnetic Resonance Imaging

Sethma Wijesinghe, Udeshika Weerathna, Christa Kovaci, Bingwen Wang, Ruchiranga Ranaweera, Matthew J. Allen, and Long Luo*



Cite This: <https://doi.org/10.1021/acsami.4c22884>



Read Online

ACCESS |



Metrics & More

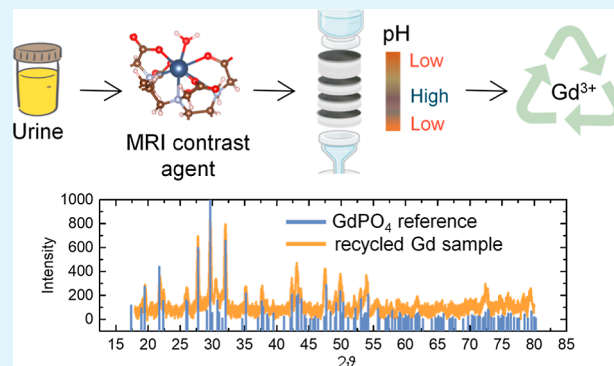


Article Recommendations



Supporting Information

ABSTRACT: The widespread use of gadolinium-based contrast agents for magnetic resonance imaging (MRI) in recent decades has led to a growing demand for Gd and raised environmental concerns due to their direct discharge into wastewater systems. In response, we developed an electrochemical filtration method to recover Gd from patient urine following contrast-enhanced MRI. This method involves modifying a conventional vacuum filtration apparatus by introducing electrodes into the filter membrane, creating a strong electric field of ~ 5 kV/m and a steep three-zone pH gradient within the filter membrane. These electric and pH fields facilitate the dissociation of Gd-based contrast agents, releasing Gd^{III} ions, electrophoretic separation of Gd^{III} and its ligand, and eventually precipitation and trapping of Gd^{III} as GdPO_4 and $\text{Gd}(\text{OH})_3$ on the filter membrane. Using gadopentetate dimeglumine (GdDTPA) as a model Gd-based contrast agent, we achieved a Gd trapping efficiency of $\sim 70\%$ for artificial and real urine samples. For macrocyclic Gd-based contrast agents such as gadoterate meglumine (GdDOTA), the Gd trapping efficiency decreased to 25.4% due to the slow dissociation kinetics of macrocyclic contrast agents. However, the trapping efficiency can be improved to $\sim 40\%$ by allowing the macrocyclic contrast agent to predissociate in an acidic environment before electrochemical filtration. The Gd trapped on the filter membrane can be recovered by thermal treatment in a muffle furnace. After thermal treatment, the reclaimed Gd from the real urine sample was primarily identified as GdPO_4 . This electrochemical filtration design offers a straightforward and practical approach to recovering Gd from contrast-enhanced MRI scans, addressing the increasing demand for Gd and helping alleviate concerns about Gd contamination in surface water.



KEYWORDS: electrochemical filtration, gadolinium recovery, magnetic resonance imaging, rare-earth element, MRI contrast agent

INTRODUCTION

Gadolinium is a rare-earth element widely used to enhance contrast in magnetic resonance imaging (MRI) due to its paramagnetic properties associated with the $^8\text{S}_{7/2}$ ground-state electronic configuration of Gd^{III} .^{1–3} The first commercial Gd-based contrast agent for MRI, gadopentetate dimeglumine (GdDTPA), was introduced in 1981.⁴ Then, Gd-based contrast agents became the primary type of contrast agents used in MRI. To date, the U.S. Food and Drug Administration has approved 12 commercial Gd-based contrast agents.^{5,6} Approximately 30 million MRI procedures involving the use of Gd-based contrast agents are performed annually.⁵ Over 450 million intravenous Gd-based contrast agent doses (approximately 1.2 g of Gd per dose, totaling over 540 tons of Gd) have been administered to millions of patients worldwide.⁷ The global demand for Gd has been steadily increasing, reaching a market value of approximately US\$5.3 billion in 2022, and it is forecast to grow to US\$8.8 billion by 2032.⁸

The Gd-based contrast agents administered intravenously are mainly removed from the body through the kidneys with a

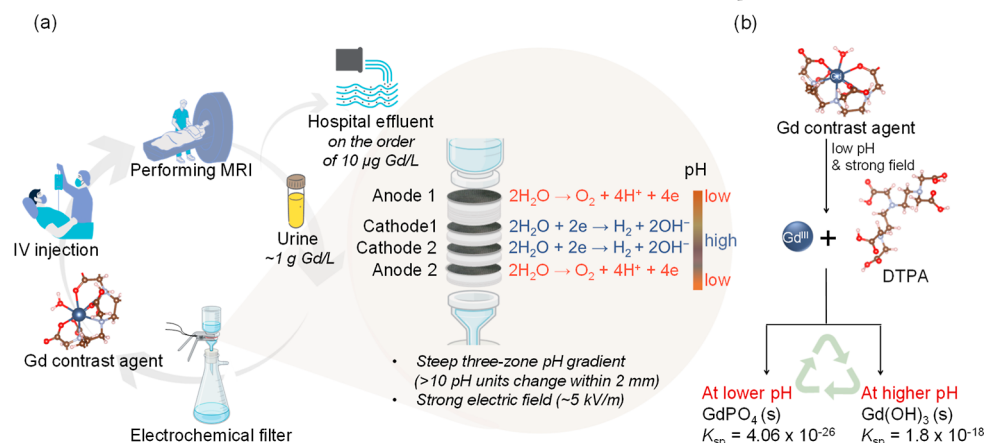
large portion being excreted in the urine without undergoing any chemical changes. In individuals with normal kidney function, about 70% of the total injected Gd is excreted during the first urination and over 90% is excreted within 24 h of administration.^{7,9,10} These excreted Gd are mostly discharged into hospital wastewater systems—only approximately 10% of the Gd is removed during wastewater treatment¹¹—posing a growing environmental concern when they enter surface waters.^{12–15} The total annual Gd emissions per MRI facility were estimated to be between 2.1 and 4.2 kg per year, leading to a potential Gd concentration of 8.5–30.1 $\mu\text{g}/\text{L}$ in its wastewater.¹⁶ A study of surface waters from various points in San Francisco Bay revealed a consistent rise in Gd levels from

Received: December 27, 2024

Revised: January 13, 2025

Accepted: January 14, 2025

Scheme 1. (a) Schematic of the Proposed Electrochemical Filtration Method for Recovering Gd from Patient Urine after MRI Scans.^a (b) Flowchart Illustrating the Dissociation of a Gd-Based Contrast Agent, Gadopentetate Dimeglumine (GdDTPA), in an Electrogenerated Low-pH Environment, Leading to Separation of Gd^{III} and Its Ligand, Followed by the Precipitation of Gd^{III} in Two Different Forms, GdPO₄ and Gd(OH)₃, Based on Solution pH and K_{sp} Values.^b



^aThe electrochemical filtration setup uses two anodes, two cathodes, and multiple layers of chromatography paper to create a steep three-zone pH gradient and a strong electric field that demetalates the Gd-containing complex in the urine and precipitates Gd for sustainable reuse. ^bThe blue, red, brown, white, and silver spheres in the molecular structures represent Gd, O, C, H, and N atoms, respectively.

8.27 to 112 pmol/kg (or 1.3 to 17 ng/L) between the early 1990s and now.¹⁷ The highest Gd anomalies were detected in locations near hospitals and research facilities using Gd-based contrast agents. Therefore, recovering Gd after MRI scans not only addresses the increasing demand for Gd but also helps address the pressing concerns about Gd contamination of surface water, which are significant and of interest to society.

Our group previously developed a ligand-assisted electrochemical aerosol formation (LEAF) process to extract and preconcentrate free Gd from hospital effluents containing a ppb level of Gd.¹⁸ We engineered amphiphilic Gd-binding ligands that spontaneously attach to the surfaces of gas bubbles. During the LEAF process, these Gd-binding ligands ride along with the electrogenerated rising bubbles and capture free Gd^{III} ions in solution. When gas bubbles reach the surface, they burst to form aerosol droplets enriched with Gd^{III}-containing complexes through a process known as aerosol enrichment.^{19–23} We demonstrated that the LEAF process extracted ~75% Gd from water samples containing a ppb level of Gd^{III} ions while preconcentrating Gd by up to ~400-fold. However, the efficiency of the LEAF process for extracting Gd from real-world hospital effluents can be affected by other metal ions, such as Fe^{III}, Zn^{II}, and Cu^{II}, that compete for Gd-binding ligands.^{16,24,25}

To overcome the limitations of the previous Gd recovery workflow, we shifted our focus to an upstream source: the urine of patients after receiving contrast-enhanced MRI scans. Recovering Gd directly from the urine of MRI patients offers two significant advantages. First, urine contains a high concentration of Gd, measuring between 48 mg/L and 21.2 g/L on the first day after exposure to Gd-based contrast agents.⁹ This concentration is considerably higher than the μg/L levels of Gd typically found in hospital wastewater.¹⁶ Second, the concentrations of multivalent metal ions, such as Zn^{II}, Ni^{II}, Cu^{II}, and Fe^{III}, are generally below 1 mg/L in healthy human urine.²⁶ This lower concentration reduces the potential interference from these metal ions, which have similar physical and chemical properties to Gd. However, unlike Gd in hospital effluents, Gd in fresh urine samples remains predominantly

(>99%) in its chelated form rather than as free ions.^{9,27} Consequently, the LEAF process, which relies on complexing amphiphilic Gd-binding ligands with free Gd^{III} ions in solution, is not effective at recovering complexed Gd from the urine.

Here, we present an electrochemical filtration method designed to directly extract Gd from patient urine following an MRI scan (Scheme 1a). We utilized water electrolysis in this electrochemical filtration system to create a significant pH gradient and a strong electric field within the filter membrane. This setup facilitates the demetalation of Gd-based contrast agents, the following electrophoretic separation of Gd^{III} from its ligand, and eventually the precipitation and trapping of Gd^{III} as GdPO₄ and Gd(OH)₃ on the filter membrane. Using GdDTPA as our model contrast agent, we demonstrated that this electrochemical filtration process achieves a Gd trapping efficiency of ~70% for both artificial and real urine samples. The filtration throughput, while maintaining optimal trapping efficiency, was about 0.60 mL of urine per minute per cm² of the filter membrane's cross-sectional area. The Gd trapped on the filter membrane can be effectively recovered through thermal treatment in a muffle furnace. Analysis of the reclaimed Gd from real urine samples revealed that it primarily existed as GdPO₄, as determined by techniques, including X-ray photoelectron spectroscopy (XPS), X-ray diffraction (XRD), and scanning electron microscopy with energy-dispersive X-ray spectroscopy (SEM/EDX).

RESULTS AND DISCUSSION

Electrochemical Filtration Device Design. According to previous speciation analyses of Gd in MRI patients' urine,^{9,27} Gd remains primarily (>99%) in its chelated form in fresh urine samples. Gd-based contrast agent complexes generally exhibit high thermodynamic stability at physiological pH levels but dissociate in strong acids. For instance, the conditional stability constant of GdDTPA at pH 7.4 is 10⁷;^{7,17} however, its dissociation half-life in 0.1 N HCl can be as short as 10 min.^{28,29} These Gd-based contrast agent complexes can dissociate when a strong acid is added to urine, allowing some Gd to precipitate as GdPO₄ at the bottom of the

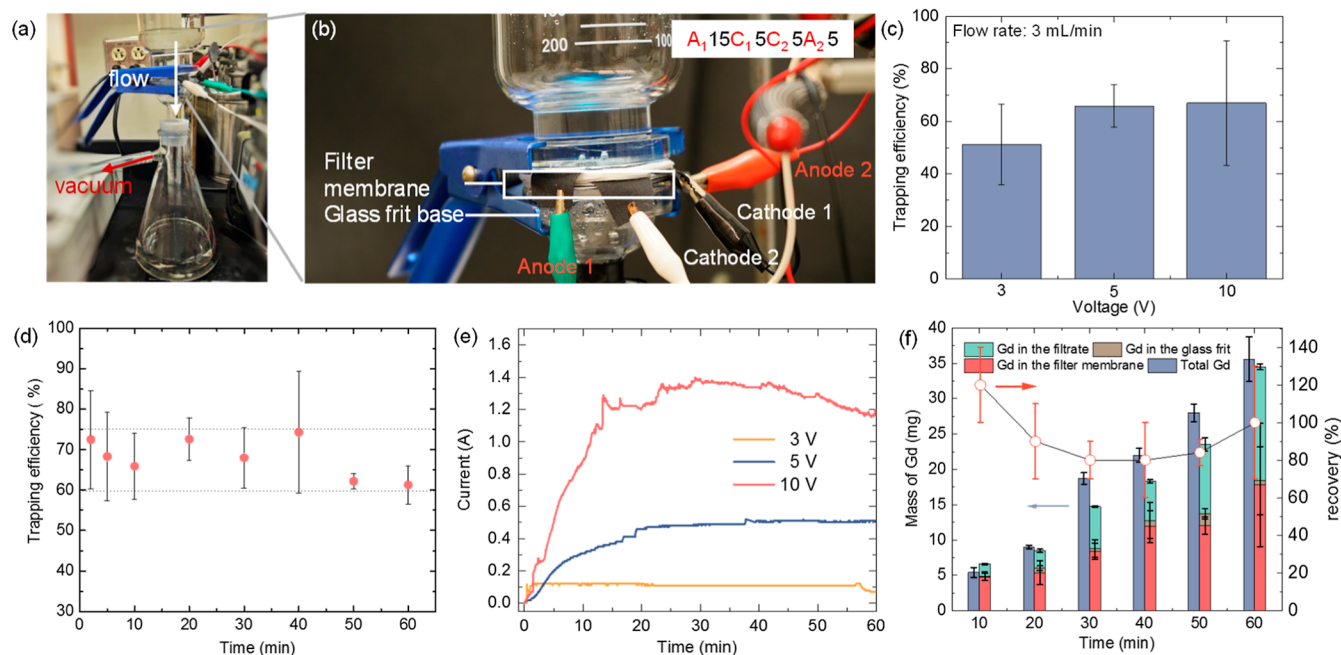


Figure 1. Photographs of (a) our electrochemical filtration system and (b) an expanded view of the optimal filter membrane structure of $A_115C_15C_25A_25$, which has 15 layers of paper between anode 1 (A1) and cathode 1 (C1), 5 layers between cathode 1 (C1) and cathode 2 (C2), and 5 layers after anode 2 (A2). (c) Comparison between the Gd trapping efficiencies at various operating voltages of 3, 5, and 10 V for GdDTPA (1 mM, 0.16 g Gd/L) in artificial urine. Flow rate: 3 mL/min and filtration time: 10 min. (d) Time-dependent Gd trapping efficiency at 5 V. (e) Current–time traces recorded during electrochemical filtration at 3, 5, and 10 V. (f) Gd mass balance analysis (left axis) and the Gd recovery (right axis) for different filtration times from 10 to 60 min. The error bars for the mass balance study and trapping efficiency were obtained from the standard deviation of three independent experiments, and the error bars for the Gd recovery were calculated from the mass balance results based on the propagation of error rules.

container due to phosphate ions in the urine. The precipitated $GdPO_4$ can be reclaimed by filtration—however, the use of strong acids and the resulting acidic waste present significant drawbacks, making this recovering approach nonideal for use in hospitals.

The electrochemical filtration design in Scheme 1a addresses this limitation. In this design, we modified a conventional vacuum filtration setup by introducing four porous carbon cloth electrodes (from top to bottom: anode 1, cathode 1, cathode 2, and anode 2) separated by filtering materials such as chromatography paper. A voltage bias of 3 to 10 V was applied between anodes and cathodes to drive water oxidation and reduction to generate H^+ and OH^- locally (Figure S2), establishing a three-zone pH gradient from low pH to high pH and back to low pH within the filter membrane. Meanwhile, a strong electric field of ~ 5 kV/m is also created between the anode and cathode due to their small separation of ~ 2 mm.^{30,31} The steep pH gradient and strong electric field in the filter membrane are essential for the removal of Gd from urine by electrochemical filtration.

The low-pH zone generated by anode 1 drives the dissociation of GdDTPA, to release Gd^{III} ions and DTPA as it passes through the filter membrane (Scheme 1b). Normally, if the ligand releases Gd^{III} ions, it would quickly rebind that same ion as the pH increases. However, this issue is overcome by the electrophoretic separation of Gd^{III} ions and DTPA enabled by the strong electric field between anode 1 and cathode 1. Our previous study found that the electrophoretic separation between Gd^{III} and a DTPA derivative in a wet grade 1 chromatography paper channel could reach >7 paper layers after 3 min in an electric field strength of ~ 16 kV/m.¹⁸ As a

result, spatial separation between free Gd^{III} ions and DTPA inhibited their recombination as they entered the high-pH zone produced by cathode 1 and cathode 2, enabling Gd^{III} to precipitate as $Gd(OH)_3$ and $GdPO_4$ due to their insolubility in alkaline media (K_{sp} for $Gd(OH)_3$ and $GdPO_4$ are 1.8×10^{-18} and 4.06×10^{-26} , respectively).^{32,33} Anode 2 was designed as an auxiliary electrode for cathode 2 to sustain the high-pH zone.

Extraction of Gd from Artificial Urine. We first tested the electrochemical filtration performance using GdDTPA (1 mM, 0.16 g of Gd/L) spiked in an artificial urine solution. Artificial urine was prepared following a reported procedure and contained KCl (60.4 mM), NaCl (128.3 mM), NaH_2PO_4 (40.0 mM), and urea (60.1 mM).³⁴ The pH of the artificial urine samples was adjusted to ~ 5 , which falls in the normal pH range of 4.5–8 in human urine.³⁵ Trapping efficiency was calculated from the remaining Gd in the filtrate and the total Gd mass passing through the filtration setup; both were measured by inductively coupled plasma mass spectrometry (ICP–MS). The Gd trapping efficiency strongly depends on the structure of the electrochemical filter membrane, which determines the pH gradient, electric field, and flow rate. We varied the arrangement and type of filter materials, including grade 1 and grade 17 chromatography paper (thickness: 0.16 and 0.8 mm per layer, respectively), hydrophilic Nylon membrane, and glass fiber membrane, as well as carbon cloth electrode materials, including plain carbon and polytetrafluoroethylene (PTFE)-treated carbon (Table S1). The optimal filter membrane structure that provides the best balance between trapping efficiency and flow rate is 15 layers of grade 1 chromatography paper between anode 1 (A1) and cathode 1

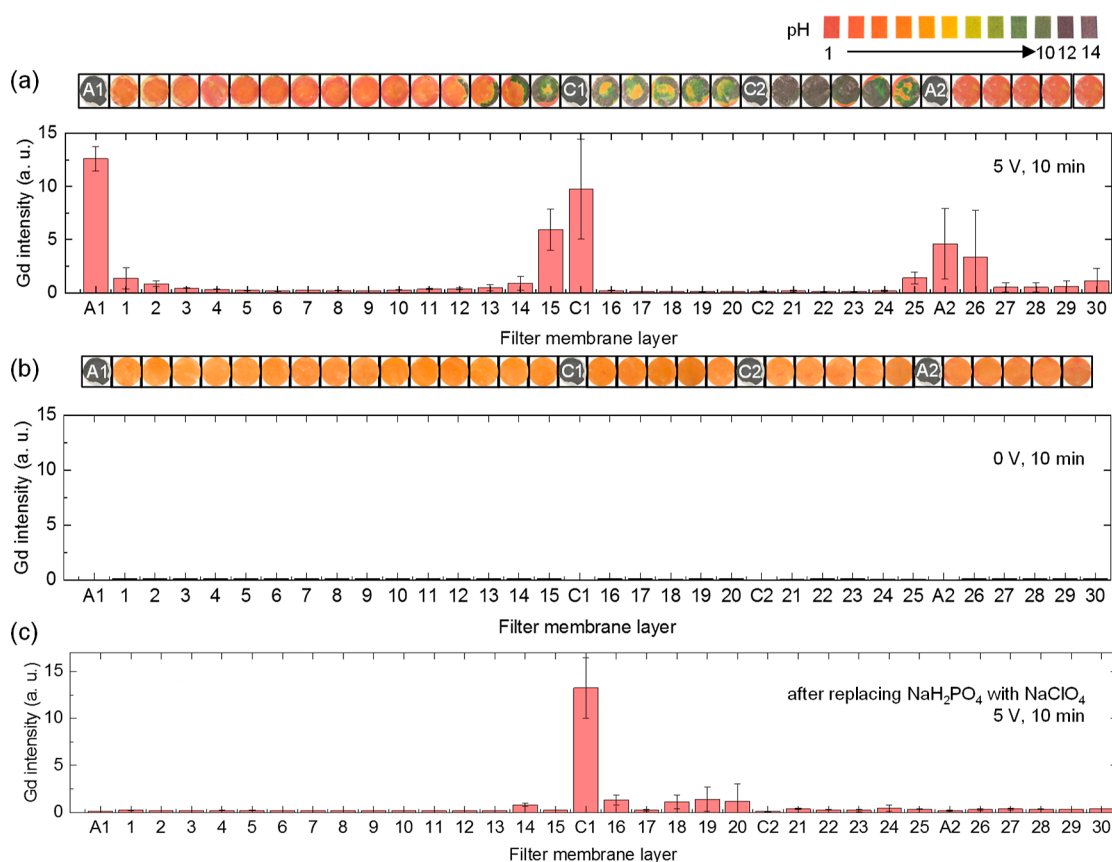


Figure 2. (a) Distributions of pH (top panel) and Gd (bottom panel) across each layer of the filter membrane after electrochemical filtration of an artificial urine sample containing GdDTPA (1 mM) at 5 V for 10 min. (b) Distributions of pH (top panel) and Gd (bottom panel) across each filter membrane layer without an applied voltage. (c) Gd distribution after electrochemical filtration of a modified artificial urine sample by replacing NaH₂PO₄ with NaClO₄ at 5 V for 10 min. The error bars are the standard deviation of the Gd content at different sampling locations of a filter membrane layer (Figure S6).

(C1), 5 layers between cathode 1 (C1) and cathode 2 (C2), and 5 layers after anode 2 (A2) (denoted by A₁15C₁5C₂5A₂5, Figure 1a,b). All the electrodes were plain carbon cloth, and the filter material was grade 1 chromatography paper with a total thickness of 6.05 mm (Figure S1).

Replacing the plain carbon cloth electrodes with PTFE-treated carbon cloth electrodes reduced the trapping efficiency and flow rate by 50% due to its hydrophobicity (entry 2 in Table S1). Strong acid treatment of the PTFE-treated carbon cloth electrodes using concentrated H₂SO₄ and HNO₃ improves the hydrophilicity (Figure S3) but did not lead to a better trapping efficiency than plain carbon electrodes (entries 11 and 14–16 in Table S1). Neither a hydrophilic Nylon nor glass fiber membrane did (entries 3 and 4 in Table S1), despite the latter having a higher flow rate than grade 1 chromatography paper (10.3 mL/min vs 3.9 mL/min). Grade 17 chromatography paper improved the trapping efficiency from 66% to 80% but sacrificed the flow rate from 3.9 to 0.5 mL/min by 87%, compared to grade 1 paper (entry 5 in Table S1), which octuples the filtration time for processing the same sample volume. Using one pair of anode and cathode instead of two pairs compromised the trapping efficiency as well (entries 9 and 10 in Table S1).

Figure 1c shows the Gd trapping efficiency after applications of 3, 5, and 10 V for 10 min using the optimal filter membrane structure. During the experiments, the flow rate was kept at ~3 mL/min, so the average residence time of the Gd-containing

sample in the filter membrane was ~1 min. We observed trapping efficiencies of >50% at all three voltages and achieved the highest efficiency of ~70% at 5 and 10 V. The error bar at 10 V was larger than 5 V because the filter paper was burned after operating for about 30 min at 10 V due to Joule heating (Figure S7). Therefore, 5 V was used for all of the other experiments. At 5 V, the Gd trapping efficiency of filtrations performed for 10 to 40 min was ~65 to 75%, with a slight decrease to 60% afterward (Figure 1d). The efficiency loss is possibly caused by the loss of mechanical integrity of filter papers or Joule heating, both of which would increase the ionic conductivity, lower the electric field in the filter membrane, and comprise the trapping efficiency, as partially supported by the gradually increasing electrical current passing between the anodes and cathodes over time (Figure 1e).

We further conducted Gd mass balance analysis by directly measuring the Gd mass in the initial artificial urine sample, in the filtrate, on the filter membrane, and inside the glass frit base of the filtration device (Figure S4). Figure 1f shows a reasonable recovery percentage of 80%–120% for filtration times from 10 to 60 min. Error bars represent the standard deviations of three independent experiments. The Gd in the filter membrane and glass frit has larger error bars than total Gd and filtrates because they are solid samples that require an extra step of Gd digestion in boiling nitric acid, resulting in greater variations. A noticeable appearance of Gd in the glass frit base from 40 min indicates the incomplete trapping of Gd

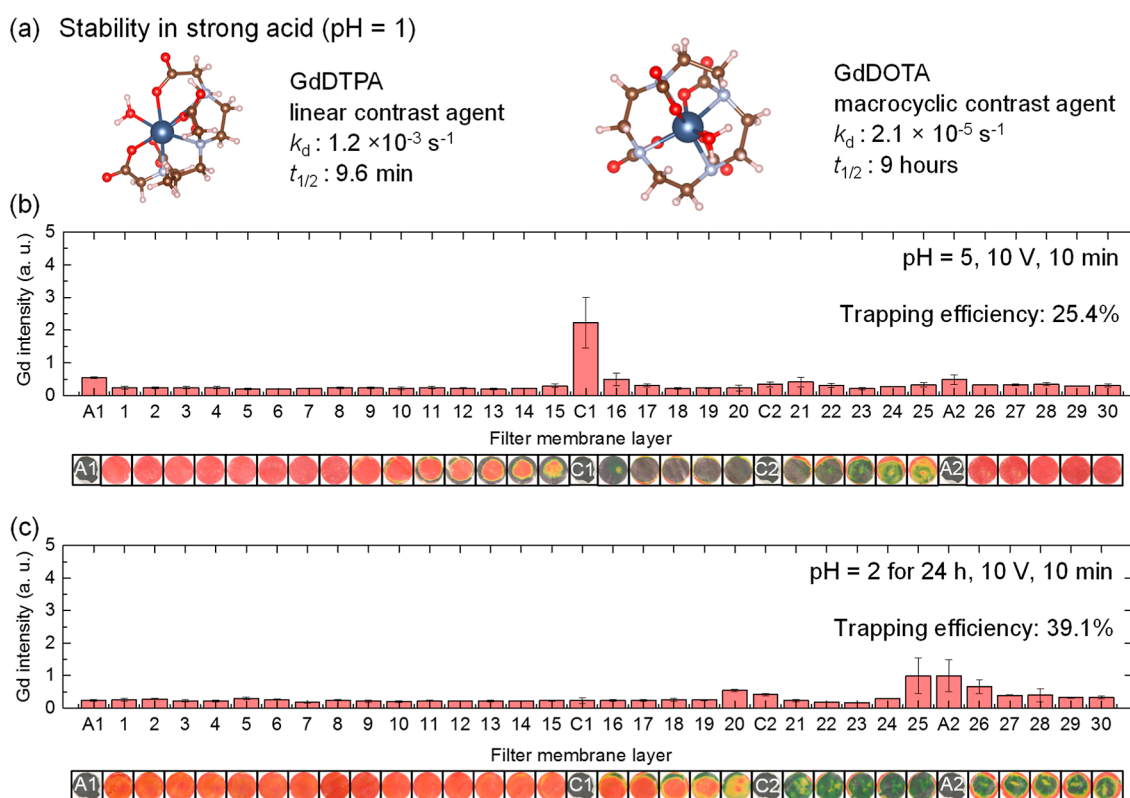


Figure 3. (a) Comparison of the stability of linear and macrocyclic contrast agents in strong acid (pH = 1). (b) Distributions of Gd (top panel) and pH (bottom panel) across each layer of the filter membrane after electrochemical filtration of an artificial urine sample containing GdDOTA (1 mM) at 10 V for 10 min. (c) Distributions of Gd (top panel) and pH (bottom panel) across each filter membrane layer for acidifying the artificial urine containing GdDOTA to pH = 2 for 24 h.

precipitates on the paper filter membrane, supporting the loss of mechanical integrity of the paper filters. The throughput of each electrochemical filtration setup is ~ 3 mL/min, and it can be scaled up by running parallel filtration. Figure S5 shows the processing of up to 95 mL of artificial urine containing GdDTPA in 10 min with an efficiency of $\sim 75\%$ using three parallel filtrations.

Next, we examined the distribution of Gd and pH across each filter membrane layer to understand the electrochemical filtration process better. We used a colorimetric assay with a universal pH indicator to measure the pH immediately after the filtration experiments, while the paper layers were still wet. The top panel of Figure 2a clearly shows three pH zones in the filter membrane after 10 min of electrochemical filtration at 5 V. Specifically, an acidic pH zone of 2 to 3 was present between A1 and C1, a neutral to basic pH zone between C1 and A2 with the highest pH value of ~ 13 on layer 22, and then another acidic pH zone of ~ 2 after A2. The transition from pH = 2 to 13 occurred in only about 10 paper layers or ~ 2 mm. It is worth noting that the diffusion of protons after the electric field and vacuum are removed should not significantly affect our pH distribution measurements because the diffusion coefficient of ions in wet filter paper is about 1/3 of their diffusion coefficient in water.³¹ This means that the diffusion coefficient of a proton in the filter membrane is around $3.1 \times 10^{-5} \text{ cm}^2/\text{s}$.³⁶ Using the 1D Einstein diffusion equation, the average diffusion time for a proton to cross one layer of filter paper with a thickness of 200 μm is estimated to be ~ 6.5 s, which is longer than the time it took us to open the layered paper membrane.

Then, we used energy-dispersive X-ray fluorescence (EDXRF) spectrometry to analyze the relative Gd content on each filter membrane layer. The bottom panel of Figure 2a displays the distribution of the average Gd $L\alpha$ line intensity in the filter membrane measured from at least three locations of each layer (Figure S6). In addition to the expected Gd deposition in the basic pH zone near C1, we also observed Gd deposition near A1 and A2 in the acidic zones. The error bars are the standard deviations of the measured Gd intensities at different locations. The relatively large error bars are due to the nonuniform pH distribution on each layer (Figure 2a) and, thus, a large variation of Gd intensity at different locations. In the absence of an applied voltage, the pH in the filter membrane was constant at ~ 5 across all of the layers, and no Gd trapping was observed for any layers (Figure 2b). Note that the carbon cloth electrodes were dark because of their native color.

To understand the origin of the presence of Gd near the anodes, we performed a control experiment using a modified artificial urine formula, in which NaH_2PO_4 was replaced with NaClO_4 at the same concentration. Under the same electrochemical filtration conditions (5 V and 10 min), the Gd trapping efficiency dropped to 27%, approximately one-third of the efficiency in the presence of phosphate salts, and Gd only appeared in the basic pH zone near C1 (Figure 2c). The difference between Figure 2a and c indicates that the trapped Gd near the cathode should be mostly $\text{Gd}(\text{OH})_3$, and Gd found near the two anodes was caused by Gd^{III} precipitating with NaH_2PO_4 or its conjugate base. The inner-sphere water of GdDTPA can be replaced with HPO_4^{2-} ,³⁷ weakening the

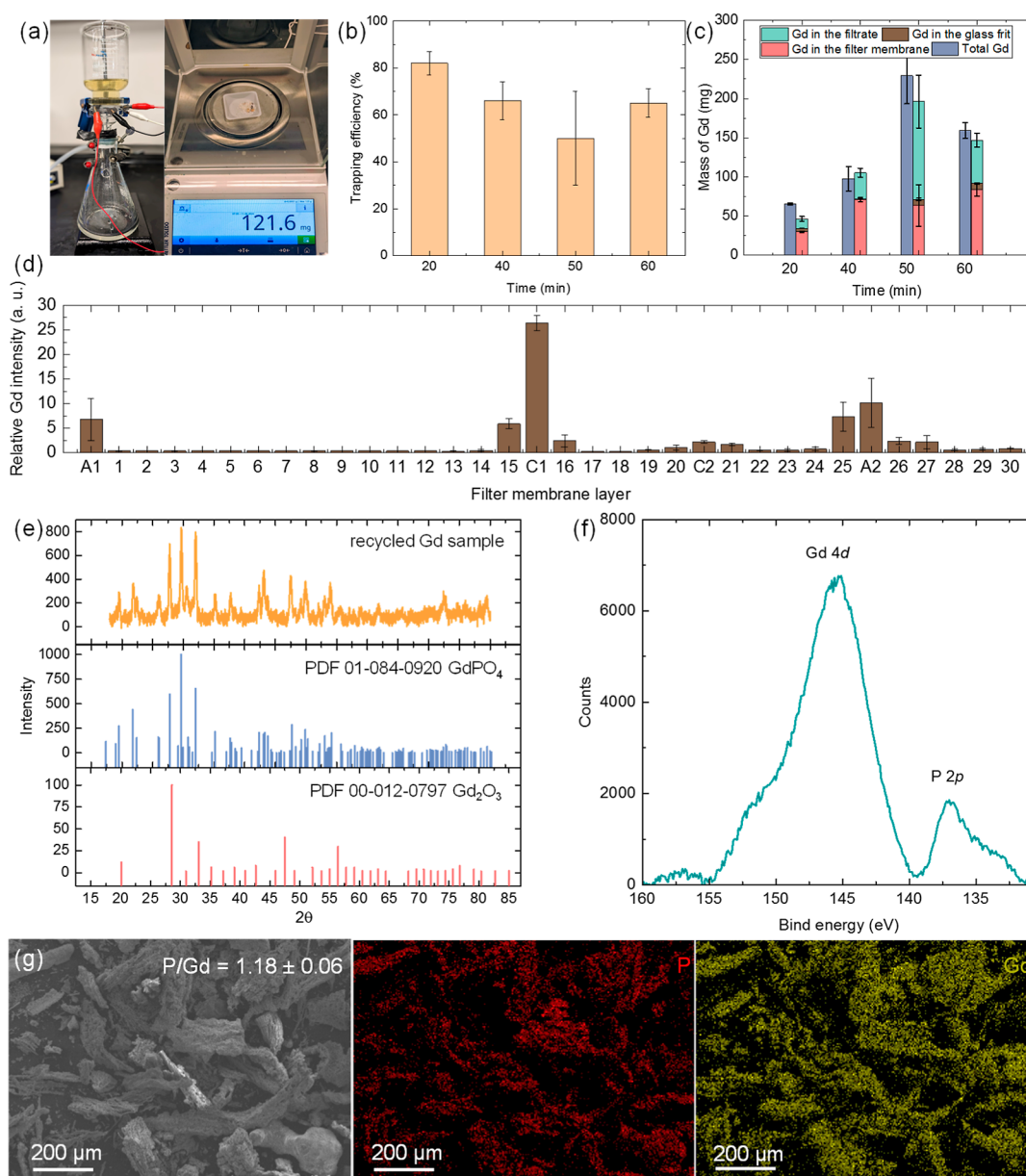


Figure 4. (a) Photographs of the experimental setup filtering real urine spiked with GdDTPA and the recovered Gd-containing particles after burning the filter membrane that trapped Gd in a muffle furnace at 1000 °C for 10 h. (b) Gd trapping efficiency and (c) mass balance analysis for four independent electrochemical filtration experiments conducted at 5 V for 20, 40, 50, and 60 min. (d) Graph showing Gd distribution on each filter membrane layer. (e) XRD patterns of the recovered Gd particles and GdPO₄ and Gd₂O₃ references. (f) XPS spectrum and (g) SEM/EDX mapping of the recovered Gd particles.

complexation and promoting the precipitation of GdPO₄ driven by its low solubility in water (14 μM), even at pH = 2.³⁸ We attempted to directly identify the presence of GdPO₄ and Gd(OH)₃ on the electrodes using XPS but did not obtain reproducible Gd and P signals (Figure S8), possibly because of the large excess of soluble phosphate salts.

Extraction of Gd from Macrocylic Gd-based Contrast Agent. In addition to the linear contrast agent GdDTPA, we tested another contrast agent, gadoterate meglumine (GdDOTA). GdDOTA belongs to the macrocylic category due to the cyclic configuration of its 2,2',2'',2'''-(1,4,7,10-tetraazacyclododecane-1,4,7,10-tetraol)tetraacetate (DOTA) ligand (Figure 3a). Compared with linear Gd-based contrast agents, macrocylic agents are more stable in acidic environments and less affected by the presence of phosphate because of the

macrocylic effect.³⁹ Figure 3a compares the dissociation rate constant (k_d) and the dissociation half-life ($t_{1/2}$, defined as the time associated with the release of Gd from half of a sample of contrast agent) of the linear and macrocylic contrast agents tested in this report at pH = 1.⁴⁰ The $t_{1/2}$ for GdDOTA is 9 h, ~60 times longer than GdDTPA's. Due to the slow dissociation of the macrocylic complex in strong acid, the Gd trapping efficiency was 25.4%, lower than the efficiency of ~70% for the linear contrast agent under the same electrochemical filtration conditions (Figure 3b). In addition, the trapped Gd was mostly present in the basic pH zone near C1, suggesting it precipitated mostly as Gd(OH)₃, consistent with the reports that macrocylic Gd-based contrast agents exhibited greater stability than linear contrast agents in the presence of phosphate.⁴¹ Despite GdDOTA's moderate

trapping efficiency, we still want to highlight that GdDOTA only experiences the electrogenerated acidic environment for less than 1 min as it flows through the filter membrane, ~ 500 times shorter than its $t_{1/2}$ measured in solution at pH 1. This difference indicates that the unique environment of a large pH gradient and strong electric field inside the filter membrane greatly accelerate the complex dissociation, which is currently under further investigation. To address the limited trapping efficiency due to slow dissociation, we adjusted the sample solution pH to 2 and held it there to promote dissociation for 24 h before electrochemical filtration. The predissociation step improved the trapping efficiency to 39.1% (Figure 3c). The trapped Gd was also found in the basic pH zone after C2. The shifted pH distribution downstream in the filter membrane is caused by the initial low pH of the sample solution, requiring OH^- produced at both C1 and C2 to be neutralized.

Extraction of Gd from Real Urine Samples. We applied our electrochemical filtration design to extract Gd from real urine samples to test its practical use. We spiked a real urine sample with GdDTPA (15 mM, 2.36 g Gd/L) to reproduce a typically observed concentration of Gd (0.048–21.2 g/L) for an MRI patient on the first day after imaging.⁹ This sample was electrochemically filtered at 5 V for up to 60 min (Figure 4a). Figure 4b shows the Gd trapping efficiency varies between 50% and 80% for different filtration times with an average trapping efficiency of $65\% \pm 13\%$, comparable to that for artificial urine samples ($\sim 70\%$). The mass balance analysis results in Figure 4c show a good Gd recovery of 71% to 108% for these experiments. However, we noticed that the flow rate through the filter membrane was not constant for the real urine samples, causing a nonlinear increase in the total Gd amount with the filtration time and an unexpected decrease at 60 min. It was possibly due to the microbial growth in urine partially blocking the flow through the filter membrane.

The Gd distribution pattern in the filter membrane was the same as that in the artificial urine experiment (Figure 4d), suggesting that Gd precipitated as $\text{Gd}(\text{OH})_3$ and GdPO_4 . After burning the filter membrane that trapped Gd after 60 min of filtration in a muffle furnace at 1000°C for 10 h, we recovered 121.6 mg of powder (Figure 4a). We characterized the powder using XRD, XPS, and SEM/EDX. Figure 4e illustrates that the XRD pattern matched best with monoclinic GdPO_4 (PDF card # 01-084-0920), which is the most stable phase of GdPO_4 after thermal annealing at over 900°C .⁴² Meanwhile, the SEM/EDX images in Figure 4g show the colocalization of Gd and P. The EDX elemental composition analysis shows a P/Gd ratio of 1.18 ± 0.06 , confirming that the recovered powder is predominantly GdPO_4 . The XPS spectrum in Figure 4f shows a Gd 4d peak at 145.4 eV and a P 2p peak at 137 eV. The spin-orbit splitting was not observed for the Gd 4d peak because the intra-atomic exchange interactions between the seven unpaired 4f electrons of Gd and the photoholes created by photoexcitation have similar energy as the spin-orbit coupling for its 4d electrons.^{43,44} As a result, complex multiplets were obtained, appearing as a broad wave in the XPS spectrum rather than a typical doublet from spin-4d orbit splitting. Analysis of the Gd 4d and P 2p peak areas in Figure 4f produced a P/Gd ratio of ~ 2.11 , a higher-than-expected value, likely caused by the presence of a trace amount of other phosphate salts such as sodium and potassium phosphates on the surface of GdPO_4 . Therefore, to the first approximation, we recovered 75.8 mg of Gd out of the total 101.5 mg of Gd (or

74.6% recovery efficiency, close to the trapping efficiency measured by ICP-MS in Figure 4b).

CONCLUSIONS

We demonstrated an electrochemical filtration method for recovering Gd from the urine. In this method, we modified a conventional vacuum filtration apparatus by introducing electrodes into the filter paper membrane to establish a strong electric field of ~ 5 kV/m and a steep three-zone pH gradient inside the filter membrane. The electric and pH fields drive the release of Gd^{III} ions, electrophoretic separation of Gd^{III} from the ligand, and precipitation and trapping of Gd^{III} as GdPO_4 and $\text{Gd}(\text{OH})_3$ on the filter membrane. We demonstrated a Gd trapping efficiency of $\sim 70\%$ for artificial and real urine samples spiked with GdDTPA. For the macrocyclic contrast agent GdDOTA, the Gd trapping efficiency was 25.4%, which is lower than that of the linear contrast agents due to the macrocyclic effect. However, the trapping efficiency was improved to $\sim 40\%$ by adding an acidic predissociation step prior to electrochemical filtration. The Gd trapped on the filter membrane can be easily recovered by thermal treatment in a muffle furnace. The reclaimed Gd from the real urine sample was identified as primarily GdPO_4 . Our electrochemical filtration design provides a straightforward and practical approach to recovering Gd from urine, addressing the increasing demand for Gd and helping address the pressing concerns about Gd contamination of surface water.

EXPERIMENTAL SECTION

Chemicals and Materials. GdDTPA (research-grade; 97%) was purchased from BenchChem. GdDOTA (research-grade; 95%) was purchased from Aaron Chemicals. A 43 element calibration standard for ICP (IV-ICPMS-71A, 10 ppm), urea (99%), potassium chloride (99%), sodium chloride (99%), sodium phosphate monobasic ($>98\%$), nitric acid (67–70%), universal indicator solution, acetic acid (99.7%), glass fiber membrane filter (0.7 μm pore size, 47 mm in diameter), Whatman cellulose chromatography papers grade 1 and grade 17 sheets (20 \times 20 cm), and polypropylene XRF thin films (1000, precut 3" \times 3" sheets) and sample cups were purchased from Sigma-Aldrich. Hydrophilic Nylon membrane filters (47 mm in diameter) were purchased from Fisher Scientific. Plain and PTFE-treated carbon cloth (26 \times 50 cm) was purchased from the Fuel Cell Store. Ultrapure water (18 M Ω cm, total organic carbon <3 ppb) was used in all aqueous solutions. Real urine samples were provided by a healthy group member.

Electrochemical Filtration. All electrochemical filtration experiments were performed using a modified laboratory vacuum filtration apparatus (see Supporting Information for details).

ICP-MS Analysis. All ICP-MS measurements were performed on an Agilent Technologies 7700 series spectrometer. All glassware, including the filtration setup, was washed in nitric acid (70% v/v) followed by ultrapure water before each experiment to dissolve any Gd^{III} attached to the glassware. For real urine samples, all urine-collecting containers were washed with nitric acid (5% v/v, 100 mL). ICP-MS samples were prepared as follows:

All samples (10 mL) were digested in boiling nitric acid (10 mL, 70% v/v) for 1 h. Then, they were cooled to ambient temperature and filtered by using a syringe filter (450 μm). Artificial urine samples were diluted 10,000 times (100 times dilution twice). Real urine samples were diluted 1,000,000 times (100 times dilution thrice). Final diluted samples were prepared in 2% nitric acid (10 mL). High matrix tune mode and the He gas mode were used for the analysis.

The calibration curve (eight points between 5 and 40 ppb) was prepared by diluting multielement standards containing Al, As, Ba, Be, Cd, Ca, Ce, Cr, Co, Cu, Dy, Er, Eu, Gd, Ga, Ho, Fe, La, Pb, Lu, Mg, Mn, Nd, Ni, P, K, Pr, Rb, Sm, Se, Ag, Na, Sr, S, Tl, Th, Tm, U, V, Yb,

Zn, Cs, B [IV-ICP-MS-71A in nitric acid (3% v/v), each of the 43 elements (10 ppm each), high-purity standards], Sc (10,000 ppm, hydrochloric acid, 10%, high-purity standards), Tb in aqueous nitric acid solution (100 ± 0.6 ppm, nitric acid, 2%, high-purity standards), and Y (9.99 ± 0.06 ppm, nitric acid, 2%, high-purity standards).

Energy-Dispersive X-ray Fluorescence. A Shimadzu EDX-7000 EDXRF spectrometer was used to analyze the filter membranes after electrochemical filtration and study the relative Gd distribution on each layer. After the filtration experiments, four disk-shaped samples (10 mm in diameter) were cut from each filter membrane and placed in a polypropylene cup with the aid of two polypropylene XRF thin films. The intensity (cps/μA) of the Gd *L*_α line was measured. Tube voltage: 50 kV; tube current: 487 μA auto; collimator: 10 mm; atmosphere: vacuum; integration time: 100 s; dead time: Max 30%.

Burning Filter Membranes Using a Muffle Furnace. After electrochemical filtration, all filter membranes were burned in the Thermo Scientific Lindberg/Blue M Moldatherm 1000 °C box furnace under the following conditions: target set point = 1000 °C, ramp rate = 10 °C/min, and dwell time = 10 h.

Powder XRD. A Bruker D2 Phaser diffractometer operated at 30 kV and 10 mA with Cu K α radiation ($\lambda = 1.5418 \text{ \AA}$) was employed. Patterns were collected in the 2θ range of 15–80° using a step size of 0.0125° and a step time of 0.5 s.

Chronoamperometry Analysis. A Riden DC power supply (Model: RD6012P) supplied a constant voltage to the filtration system. In-house software recorded the current variation at the operating voltage.

X-ray Photoelectron Spectroscopy. High-resolution P 2p and Gd 4d spectra were recorded by using a Thermo Scientific Nexsa X-ray photoelectron spectrometer with a hemispherical analyzer and monochromatic Al K α (1486.7 eV) source. All scans were recorded with a 50 eV pass energy, 0.1 eV energy step size, and 100 ms/step dwell time. Recorded spectra were analyzed using Thermo Avantage v5.9922 software. The C 1s peak at 284.8 eV was used as a reference to determine the binding energies.

■ ASSOCIATED CONTENT

SI Supporting Information

The Supporting Information is available free of charge at <https://pubs.acs.org/doi/10.1021/acsami.4c22884>.

Photographs of the optimal filter membrane, electrochemical filtration setup, optimization table for the filter membrane structure, details about ICP–MS and EDXRF analyses, and parallel filtration experiment results (PDF)

■ AUTHOR INFORMATION

Corresponding Author

Long Luo – Department of Chemistry, Wayne State University, Detroit, Michigan 48202, United States; Department of Chemistry, University of Utah, Salt Lake City, Utah 84112, United States; orcid.org/0000-0001-5771-6892; Email: long.luo@utah.edu

Authors

Sethma Wijesinghe – Department of Chemistry, Wayne State University, Detroit, Michigan 48202, United States

Udeshika Weeraratna – Department of Chemistry, Wayne State University, Detroit, Michigan 48202, United States

Christa Kovaci – Department of Chemistry, Wayne State University, Detroit, Michigan 48202, United States

Bingwen Wang – Department of Chemistry, Wayne State University, Detroit, Michigan 48202, United States

Ruchiranga Ranaweera – Department of Chemistry, Wayne State University, Detroit, Michigan 48202, United States

Matthew J. Allen – Department of Chemistry, Wayne State University, Detroit, Michigan 48202, United States; orcid.org/0000-0002-6868-8759

Complete contact information is available at: <https://pubs.acs.org/doi/10.1021/acsami.4c22884>

Author Contributions

The manuscript was written with the contributions of all authors, and all authors have approved the final version.

Notes

The authors declare no competing financial interest.

■ ACKNOWLEDGMENTS

The authors acknowledge support from the United States Army Engineer Research and Development Center (ERDC) under Cooperative Agreement Number W912HZ-21-2-0048, the Alfred P. Sloan Foundation (Grant # FH-2023-20829), the Carl R. Johnson Professorship from Wayne State University, and the startup funds from the University of Utah. This work used the UPS/XPS partially funded by the National Science Foundation #1849578, and the Talos F200X G2 S/TEM analysis is funded in part through NSF MRI award #2018587.

■ REFERENCES

- (1) Caravan, P.; Ellison, J. J.; McMurry, T. J.; Lauffer, R. B. Gadolinium(III) Chelates as MRI Contrast Agents: Structure, Dynamics, and Applications. *Chem. Rev.* **1999**, *99* (9), 2293–2352.
- (2) Woods, M.; Botta, M. *Metal-Containing Molecules and Nanomaterials From Diagnosis to Therapy*; CRC Press, 2024; Vol. 135, p 164.
- (3) Xiao, Y. D.; Paudel, R.; Liu, J.; Ma, C.; Zhang, Z. S.; Zhou, S. K. MRI contrast agents: Classification and application (Review). *Int. J. Mol. Med.* **2016**, *38* (5), 1319–1326.
- (4) Lohrke, J.; Frenzel, T.; Endrikat, J.; Alves, F. C.; Grist, T. M.; Law, M.; Lee, J. M.; Leiner, T.; Li, K. C.; Nikolaou, K.; et al. 25 Years of Contrast-Enhanced MRI: Developments, Current Challenges and Future Perspectives. *Adv. Ther.* **2016**, *33* (1), 1–28.
- (5) Pierre, V. C.; Allen, M. J.; Caravan, P. Contrast agents for MRI: 30+ years and where are we going? *J. Biol. Inorg. Chem.* **2014**, *19* (2), 127–131.
- (6) Hao, J.; Pitrou, C.; Bourrinet, P. A Comprehensive Overview of the Efficacy and Safety of Gadopipiclenol: A New Contrast Agent for MRI of the CNS and Body. *Invest. Radiol.* **2024**, *59* (2), 124–130.
- (7) McDonald, R. J.; Levine, D.; Weinreb, J.; Kanal, E.; Davenport, M. S.; Ellis, J. H.; Jacobs, P. M.; Lenkinski, R. E.; Maravilla, K. R.; Prince, M. R.; et al. Gadolinium Retention: A Research Roadmap from the 2018 NIH/ACR/RSNA Workshop on Gadolinium Chelates. *Radiology* **2018**, *289* (2), 517–534.
- (8) Gadolinium Market Overview, 2022–2032. <https://www.futuremarketinsights.com/reports/gadolinium-market>. (accessed Jan 13, 2025).
- (9) Loreti, V.; Bettmer, J. Determination of the MRI contrast agent Gd-DTPA by SEC-ICP-MS. *Anal. Bioanal. Chem.* **2004**, *379* (7–8), 1050–1054.
- (10) Weinmann, H. J.; Brasch, R. C.; Press, W. R.; Wesbey, G. E. Characteristics of gadolinium-DTPA complex: a potential NMR contrast agent. *AJR Am. J. Roentgenol.* **1984**, *142* (3), 619–624.
- (11) Telgmann, L.; Wehe, C. A.; Birka, M.; Kunemeyer, J.; Nowak, S.; Sperling, M.; Karst, U. Speciation and isotope dilution analysis of gadolinium-based contrast agents in wastewater. *Environ. Sci. Technol.* **2012**, *46* (21), 11929–11936.
- (12) Rogowska, J.; Olkowska, E.; Ratajczyk, W.; Wolska, L. Gadolinium as a new emerging contaminant of aquatic environments. *Environ. Toxicol. Chem.* **2018**, *37* (6), 1523–1534.
- (13) Ognard, J.; Barrat, J.-A.; Chazot, A.; Alavi, Z.; Ben Salem, D. Gadolinium footprint: Cradle to cradle? *Elsevier* **2020**, *47*, 247–249.

- (14) Martino, C.; Byrne, M.; Roccheri, M. C.; Chiarelli, R. Interactive effects of increased temperature and gadolinium pollution in *Paracentrotus lividus* sea urchin embryos: a climate change perspective. *Aquat. Toxicol.* **2021**, *232*, 105750.
- (15) Brunjes, R.; Hofmann, T. Anthropogenic gadolinium in freshwater and drinking water systems. *Water Res.* **2020**, *182*, 115966.
- (16) Kümmerer, K.; Helmers, E. Hospital Effluents as a Source of Gadolinium in the Aquatic Environment. *Environ. Sci. Technol.* **2000**, *34* (4), 573–577.
- (17) Hatje, V.; Bruland, K. W.; Flegal, A. R. Increases in Anthropogenic Gadolinium Anomalies and Rare Earth Element Concentrations in San Francisco Bay over a 20 Year Record. *Environ. Sci. Technol.* **2016**, *50* (8), 4159–4168.
- (18) Ranaweera, R.; Wijesinghe, S.; Weeraratna, U.; Chowdhury, A.; Kajjam, A. B.; Wang, B.; Dittrich, T. M.; Allen, M. J.; Luo, L. Recycling Gadolinium from Hospital Effluent via Electrochemical Aerosol Formation. *ACS ES&T Eng.* **2024**, *4* (3), 540–549.
- (19) Gantt, B.; Meskhidze, N. The physical and chemical characteristics of marine primary organic aerosol: a review. *Atmos. Chem. Phys.* **2013**, *13* (8), 3979–3996.
- (20) Wilson, T. W.; Ladino, L. A.; Alpert, P. A.; Breckels, M. N.; Brooks, I. M.; Browse, J.; Burrows, S. M.; Carslaw, K. S.; Huffman, J. A.; Judd, C.; et al. A marine biogenic source of atmospheric ice-nucleating particles. *Nature* **2015**, *525* (7568), 234–238.
- (21) An, S.; Ranaweera, R.; Luo, L. Harnessing bubble behaviors for developing new analytical strategies. *Analyst* **2020**, *145* (24), 7782–7795.
- (22) Cao, Y.; Lee, C.; Davis, E. T. J.; Si, W.; Wang, F.; Trimpin, S.; Luo, L. 1000-Fold Preconcentration of Per- and Polyfluorinated Alkyl Substances within 10 minutes via Electrochemical Aerosol Formation. *Anal. Chem.* **2019**, *91* (22), 14352–14358.
- (23) McMurdo, C. J.; Ellis, D. A.; Webster, E.; Butler, J.; Christensen, R. D.; Reid, L. K. Aerosol enrichment of the surfactant PFO and mediation of the water–air transport of gaseous PFOA. *Environ. Sci. Technol.* **2008**, *42* (11), 3969–3974.
- (24) Bau, M.; Dulski, P. Anthropogenic origin of positive gadolinium anomalies in river waters. *Earth Planet. Sci. Lett.* **1996**, *143* (1), 245–255.
- (25) Puttagunta, N. R.; Gibby, W. A.; Puttagunta, V. L. Comparative transmetallation kinetics and thermodynamic stability of gadolinium-DTPA bis-glucosamide and other magnetic resonance imaging contrast media. *Invest. Radiol.* **1996**, *31* (10), 619–624.
- (26) Zhang, Z.; Guo, S.; Hua, L.; Wang, B.; Chen, Q.; Liu, L.; Xiang, L.; Sun, H.; Zhao, H. Urinary Levels of 14 Metal Elements in General Population: A Region-Based Exploratory Study in China. *Toxics* **2023**, *11* (6), 488.
- (27) Silva, M. F.; Olsina, R. A.; Olsina, R. A. Monitoring the elimination of gadolinium-based pharmaceuticals. Cloud point preconcentration and spectrophotometric determination of Gd(III)-2-(3,5-dichloro-2-pyridylazo)-5-dimethylaminophenol in urine. *Analyst* **1998**, *123* (9), 1803–1807.
- (28) Ersoy, H.; Rybicki, F. J. Biochemical safety profiles of gadolinium-based extracellular contrast agents and nephrogenic systemic fibrosis. *J. Magn. Reson. Imaging* **2007**, *26* (5), 1190–1197.
- (29) Cacheris, W. P.; Quay, S. C.; Rocklage, S. M. The relationship between thermodynamics and the toxicity of gadolinium complexes. *Magn. Reson. Imaging* **1990**, *8* (4), 467–481.
- (30) Li, X.; Luo, L.; Crooks, R. M. Low-voltage paper isotachopheresis device for DNA focusing. *Lab Chip* **2015**, *15* (20), 4090–4098.
- (31) Luo, L.; Li, X.; Crooks, R. M. Low-voltage origami-paper-based electrophoretic device for rapid protein separation. *Anal. Chem.* **2014**, *86* (24), 12390–12397.
- (32) Djurdjevic, P.; Jelic, R.; Joksovic, L.; Lazarevic, I.; Jelick-Stankov, M. Study of Solution Equilibria Between Gadolinium(III) Ion and Moxifloxacin. *Acta Chim. Slov.* **2010**, *57* (2), 386–397.
- (33) Gysi, A. P.; Harlov, D.; Miron, G. D. The solubility of monazite (CePO₄), SmPO₄, and GdPO₄ in aqueous solutions from 100 to 250 °C. *Geochim. Cosmochim. Acta* **2018**, *242*, 143–164.
- (34) Shmaefsky, B. Artificial Urine for Laboratory Testing: Revisited. *Am. Biol. Teach.* **1995**, *57* (7), 428–430.
- (35) Sarigul, N.; Korkmaz, F.; Kurultak, I. A New Artificial Urine Protocol to Better Imitate Human Urine. *Sci. Rep.* **2019**, *9* (1), 20159.
- (36) Amdursky, N.; Lin, Y.; Aho, N.; Groenhof, G. Exploring fast proton transfer events associated with lateral proton diffusion on the surface of membranes. *Proc. Natl. Acad. Sci. U.S.A.* **2019**, *116* (7), 2443–2451.
- (37) Gao, S.; George, S. J.; Zhou, Z. H. Interaction of Gd-DTPA with phosphate and phosphite: toward the reaction intermediate in nephrogenic systemic fibrosis. *Dalton Trans.* **2016**, *45* (12), 5388–5394.
- (38) Poitrasson, F.; Oelkers, E.; Schott, J.; Montel, J.-M. Experimental determination of synthetic NdPO₄ monazite end-member solubility in water from 21 °C to 300 °C: implications for rare earth element mobility in crustal fluids. *Geochim. Cosmochim. Acta* **2004**, *68* (10), 2207–2221.
- (39) Chehabeddine, L.; Al Saleh, T.; Baalbaki, M.; Saleh, E.; Houry, S. J.; Hannoun, S. Cumulative administrations of gadolinium-based contrast agents: risks of accumulation and toxicity of linear vs macrocyclic agents. *Crit. Rev. Toxicol.* **2019**, *49* (3), 262–279.
- (40) Sherry, A. D.; Caravan, P.; Lenkinski, R. E. Primer on gadolinium chemistry. *J. Magn. Reson. Imaging* **2009**, *30* (6), 1240–1248.
- (41) Frenzel, T.; Lengsfeld, P.; Schirmer, H.; Hutter, J.; Weinmann, H. J. Stability of gadolinium-based magnetic resonance imaging contrast agents in human serum at 37 degrees C. *Invest. Radiol.* **2008**, *43* (12), 817–828.
- (42) Janulevicius, M.; Klimkevicius, V.; Mikoliunaite, L.; Vengalis, B.; Vargalis, R.; Sakirzanovas, S.; Plausinaitiene, V.; Zilinskas, A.; Katelnikovas, A. Ultralight Magnetic Nanofibrous GdPO₄(4) Aerogel. *ACS Omega* **2020**, *5* (23), 14180–14185.
- (43) Szade, J.; Neumann, M.; Karla, I.; Schneider, B.; Fangmeyer, F.; Matteucci, M. Photon energy dependence of the Gd 4d photoemission. *Solid State Commun.* **2000**, *113* (12), 709–712.
- (44) Zatsepin, D. A.; Boukhalov, D. W.; Zatsepin, A. F.; Kuznetsova, Y. A.; Mashkovtsev, M. A.; Rychkov, V. N.; Shur, V. Y.; Esin, A. A.; Kurmaev, E. Z. Electronic structure, charge transfer, and intrinsic luminescence of gadolinium oxide nanoparticles: Experiment and theory. *Appl. Surf. Sci.* **2018**, *436*, 697–707.